IEREK PRESS
Academic Research Community

http://www.press.ierek.com

ARChive

CrossMark

ISSN (Print: 2537-0154, online: 2537-0162)

International Journal on:

The Academic Research Community Publication

DOI: 10.21625/archive.v3i1.446

Battery Charging Application with Thermoelectric Generators as Energy Harvesters

Zakariya M. Dalala[1], Zaid S. Hamdan[1], Hussein Al-Taani[2], Mohammad Al-Addous[1], Aiman Albatayneh[1]

[1]*Energy Engineering Department German Jordanian University P.O. Box 35247 Amman, Jordan*

[2]*School of Basic Sciences and Humanities, German Jordanian University, Amman, Jordan*

Abstract

This paper discusses and presents the implementation of a boost converter as power electronic interface to be used with the thermoelectric generator (TEG). The common application for such system is the battery charger. The boundary conditions for battery chargers include the charging current and battery voltage limits which have to be respected throughout the charging process, while the maximization of the power generated from the TEG is a global target that is desired to be met as much as possible. Coordinated control algorithm that collectively combines these constraints is the main focus of this work. Novel global control algorithm is proposed and verified in this paper with detailed analysis that shows the effectiveness of the proposed algorithm. Dual control loops for the voltage and current of the boost converter will be designed and analyzed to satisfy the source and load demands. Maximum power point tracking (MPPT) mode, power matching mode and voltage stabilization mode will be integrated in the control algorithm of the battery charger. This paper puts a schematic design for a system that harvests energy from a thermoelectric generator bank of a TEG1-12611-6.0 TEG modules in order to charge a battery bank of Samsung ICR18650 Batteries using constant current (CC) and constant voltage (CV) charging profiles.

Keywords

Battery Charger; Boost Converter; Thermoelectric Generator; Li-Ion Battery; MPPT; Perturb and Observe

1. Introduction

Energy's importance has increased with the great population increase and prosperity linked with the advances in technology and industrial automation, which by itself has increased and diversified energy consumption. This has led to oil shortages and higher prices. The idea of alternative energy gained attention for the first time during the energy crisis of 1974, which led to igniting a serious research for alternative energy solutions, opening the door for nuclear energy as a reliable alternative to oil in some countries such as France. Energy saving regulations have also been issued and approved afterwards to manage the energy sector in more optimized manner.

Another problem that has arose over the last decades, is the climate change that is causing many natural disasters and extreme weather conditions. Many studies state that the greenhouse gasses (GHGs) emissions mostly produced by burning fossil fuels is the cause of this problem, which is forcing governments to cooperate to regulate these

emissions[1]. Nuclear energy has its own dangers, the Chernobyl and Fukushima incidents for example, in addition to the radioactive wastes make this option not too attractive. This led to increased interest in solar, wind and wave energy as possible alternative sources [2]. In addition to renewable energy resources utilization, such as wind and solar, huge attention has been paid as well to the energy efficiency related research. As most of the wasted energy in the world nowadays is mostly thermal, techniques and measures have been proposed to enhance the thermal cycles' efficiency and to shorten the energy conversion sequence to guarantee best efficiency attainable. Heat engines are extreme and very versatile example of industrial tool vastly used today and efficiency tuning is imminent in these systems.

The major problem of the heat engine – which is the base of transportation and electricity generation, is its low efficiency. About one third of energy input is converted to work and two thirds are waste heat. This cannot be eliminated or magnificently reduced according to Carnot efficiency rule, which states that the maximum possible efficiency of the heat engine is governed by the hot and cold media temperatures. By simple calculation, the ideal efficiency is around 60%, this waste heat can be an auxiliary energy source to improve the overall system's performance. Many researches addressed recovering this energy in what is called "Waste Heat Recovery (WHR)" One example for waste heat recovery, is the use of combined cycle, i.e. using Brayton (Gas turbine) with a Rankine (Steam turbine) for electric generation, during which the heat is extracted from the exhaust of the gas turbine to evaporate the water to start the steam turbine. This method increases the overall system efficiency to a value of 60% in some applications [3].

The thermoelectric generators (TEG) perfectly can be used as well as energy harvesters to scavenge energy from wasted heat [4]. The TEGs are solid-state devices engineered to generate electricity directly from heat, what is known as Seebeck effect [5]. The temperature gradient across the structure has to be maintained to generate lucrative amount of electrical energy that can be used to charge batteries for example or to support a load. Traditional usage of TEGs has been in the fields of specialized military, medical and some space applications due to their reported low efficiency [6]. Nowadays, and due to increased systems' efficiency requirements and declining prices of TEG manufacturing, more diverse applications have been found for energy harvesting with TEG as core conversion unit [7, 8].

In this manuscript, a battery charger circuit design and control is proposed for use with TEG as energy harvester. A boost converter is chosen as DC/DC converter. Critical control objectives for battery chargers are the charging current and voltage limits which have to be respected for specific type of batteries. Maximum power point tracking (MPPT) is essential when operating TEG conversion circuits, however, engaging MPPT should take place while the charging current is below suggested limit by the battery manufacturer. Seamless transition between MPPT control mode and constant voltage/current modes is implemented in the proposed control algorithm to guarantee optimum operation while meeting the boundary conditions of the operations limits.

2. System Structure

The proposed system consists of the TEG bank, the battery bank and the power conditioner which is a DC-DC boost converter and the control circuit as shown in the Fig. 1.

The TEG model is simply a voltage source that represents the open circuit voltage connected to a series resistance as shown in Fig. 2. The values of the voltage and resistance depend on the temperature difference between the hot and cold sides of the TEG.

The TEG bank used in the system consists of 20 modules of TEG1-12611-6.0 commercial product. From the datasheet, it works in the hot side temperature range of 50 – 300 ^{o}C, but in the design the range is 100 – 200^{o}C and keeping the cold side temperature fixed to 30^{o}C by cooling, giving voltage range of 5.2 – 12 V. The TEG is modeled using PSIM software, and the modeling equations are obtained by curve fitting methods applied to the voltage and power curves of the TEG. Fig. 3 shows the specifications of the TEG1-12611-6 module.

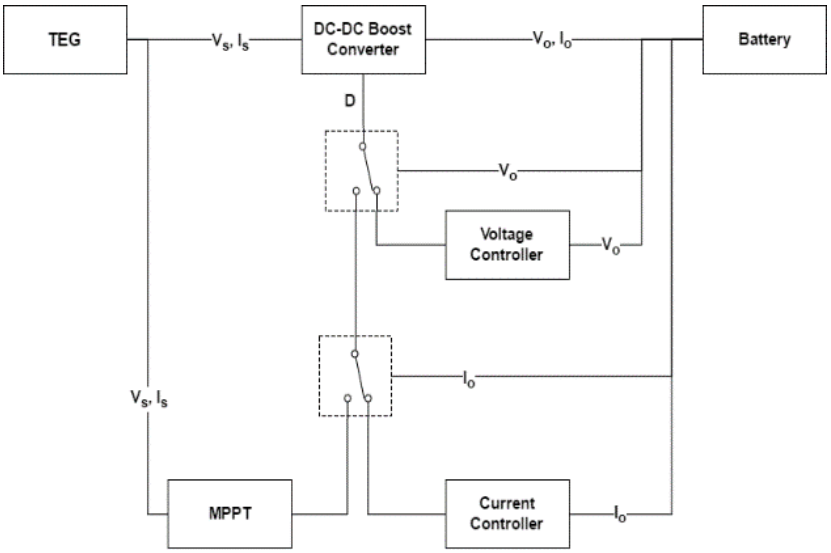

Figure 1. Proposed system block diagram

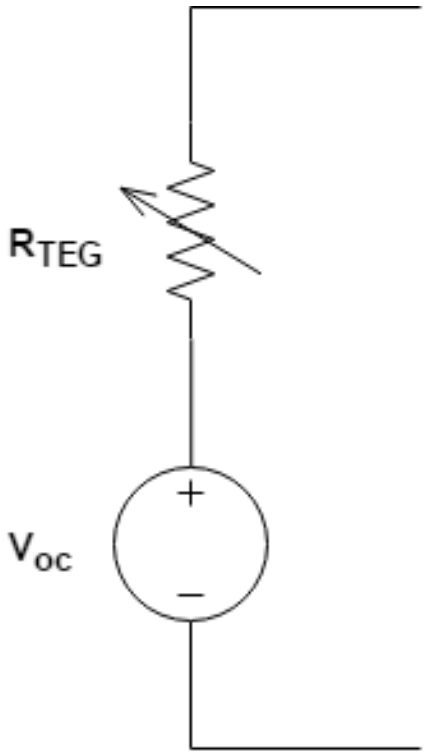

Figure 2. Thermoelectric generator equivalent circuit

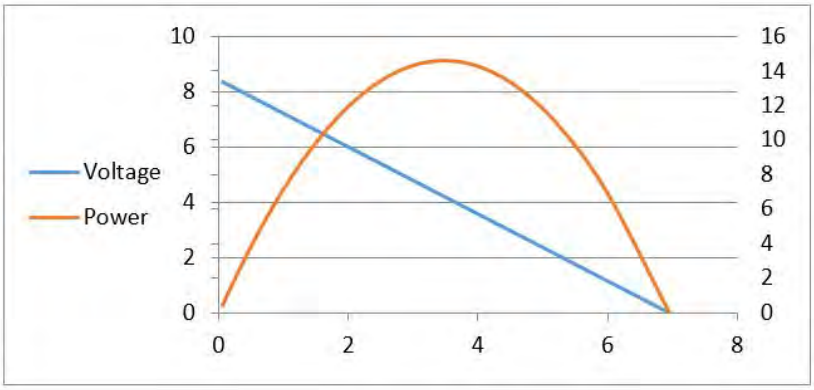

Figure 3. TEG1-12611-6.0Module specifications

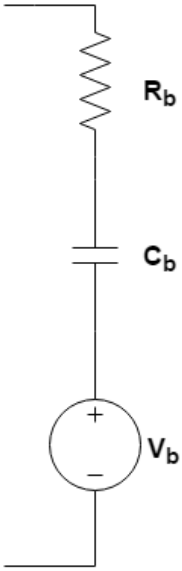

Figure 4. Battery equivalent circuit

The battery model is simply a large capacitor connected in series with a resistor, in addition to a voltage source to represent the open circuit voltage of the battery as in Fig. 4. Reference [9] developed this model for the battery when charged by constant current/ constant voltage charging profiles, and calculate the values of Cb and Rb.

The Topology of the converter used is the boost converter, the converter design takes into consideration the wide range of power input and the maximum power transfer. The converter is connected to an output inductor for further smoothing of the charging current as shown in the Fig. 5. The output inductor is introduced for fine control and ripple elimination of the charging current.

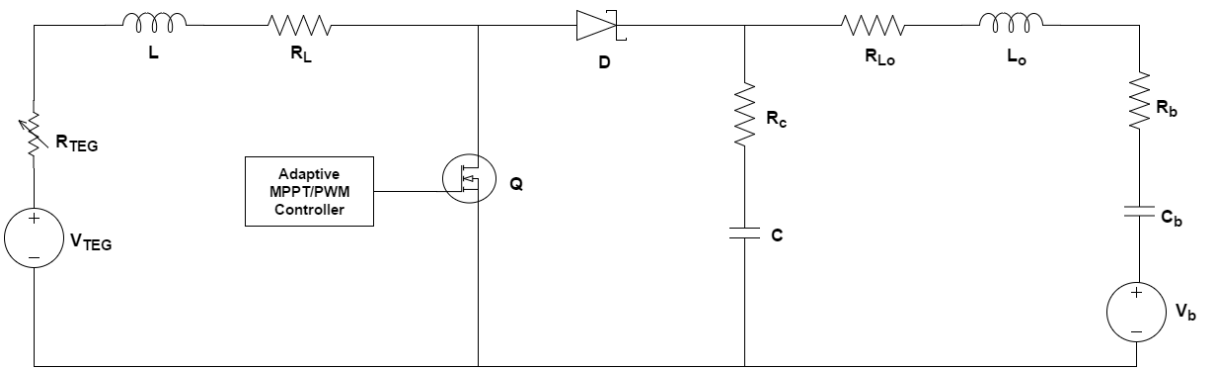

Figure 5. Proposed system circuit

The output inductor design process is carried out side by side with the output capacitor design for desired ripple in the output voltage and current. In [10], the values of output capacitor and output inductor are given by equations (1) and (2).

$$C_o = \frac{2(1-D)T(\sqrt{\triangle v_o + \frac{\triangle i_o I_o D R_{parasitic}}{1-D}} - \triangle v_o)}{\triangle i_o R^2_{parasitic}} \tag{1}$$

$$L_o = \frac{R^2_{parastic}}{4} \times \frac{2(1-D)T(\sqrt{\triangle v_o + \frac{\triangle i_o I_o D R_{parasitic}}{1-D}} - \triangle v_o)}{\triangle i_o R^2_{parasitic}} \tag{2}$$

Where $R_{parasitic} = R_b + R_c + R_{Lo}, \triangle v_o$ *and* $\triangle i_o$ re the output voltage and current ripples respectively. For the controller, an adaptive control scheme is used by combining the MPPT Perturb and Observe (P&O) controller with the simple current and voltage controller to perform the constant current/constant voltage charging profile with MPPT, as shown in the Fig.1 above. The Perturb and Observe (P&O) algorithm is shown in the Fig. 6 [11].

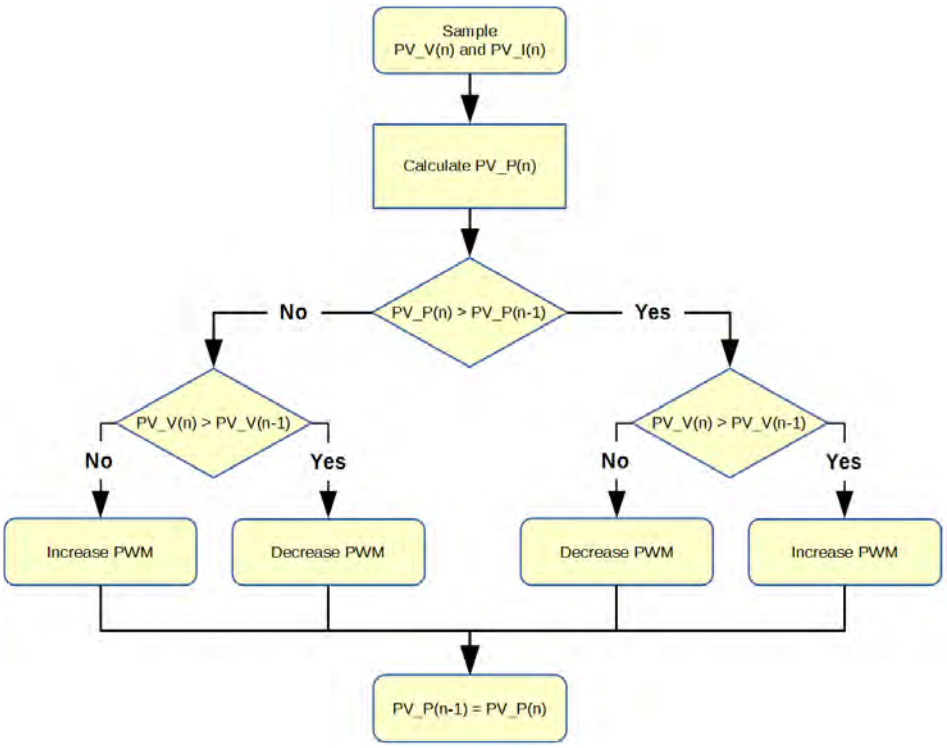

Figure 6. Perturb and Observe MPPT algorithm

3. Modeling and Controller Design

For the voltage and current controller, the duty cycle to output current, $\frac{i}{d}$ and the duty cycle to output voltage, $\frac{\hat{v_o}}{d}$ transfer functions are calculated using the PWM switch model [12], the system's small signal model is in Fig. 7. And the transfer functions are shown in equations (3) and (12).

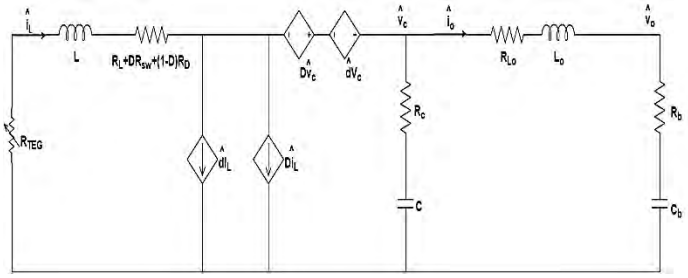

Figure 7. Small signal model of the system

$$\frac{\hat{v_o}}{d} = \frac{V_o h(1-D) + \frac{hR_{Lo}}{R_b}(1-D)(V_o - V_b) - \frac{h(R_1+sL)}{R_b(1-D)}(V_o - V_b)}{a_4 s^4 + a_3 s^3 + a_2 s^2 + a_1 s + a_0} \tag{3}$$

Where:

$$I_o = \frac{V_o - V_b}{R_b} \tag{4}$$

$$I_L = \frac{I_o}{1-D} = \frac{V_o - V_b}{R_b(1-D)} \tag{5}$$

$$h = s^2 C C_b R_c R_b + s(C_b R_b + C R_c) + 1 \tag{6}$$

$$a_4 = L L_o C C_b \tag{7}$$

$$a_3 = L C C_b (R_b + R_c + R_{Lo}) + L_o C C_b (R_1 + R_c (1-D)^2) \tag{8}$$

$$a_2 = L(C + C_b) + C C_b R_1 (R_b + R_{Lo} + R_c) + (C C_b R_c (R_b + R_{Lo}) + L_o C_b) \times (1-D)^2 \tag{9}$$

$$a_1 = R_1 (C + C_b) + (1-D)^2 \times (C R_c + C_b (R_{Lo} + R_b)) \tag{10}$$

$$a_o = (1-D)^2 \tag{11}$$

For the output current transfer function:

$$\hat{d} = \frac{\hat{v_o}}{d} \times \frac{1}{R_b} = \frac{1}{R_b} \times h \times \frac{(V_b + I_o(R_b + R_{Lo})) \times (1-D) - \frac{I_o}{1-D}(R_1 + sL)}{a_4 s^4 + a_3 s^3 + a_2 s^2 + a_1 s + a_0} \tag{12}$$

The responses and margins of stability are shown in Fig. 8. and Fig. 9.

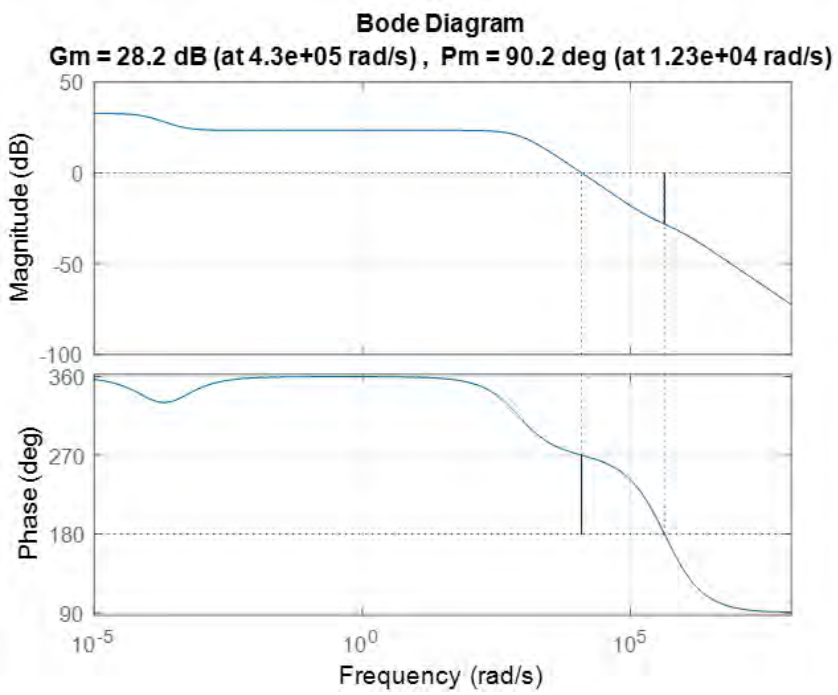

Figure 8. Bode plot of the output voltage transfer function

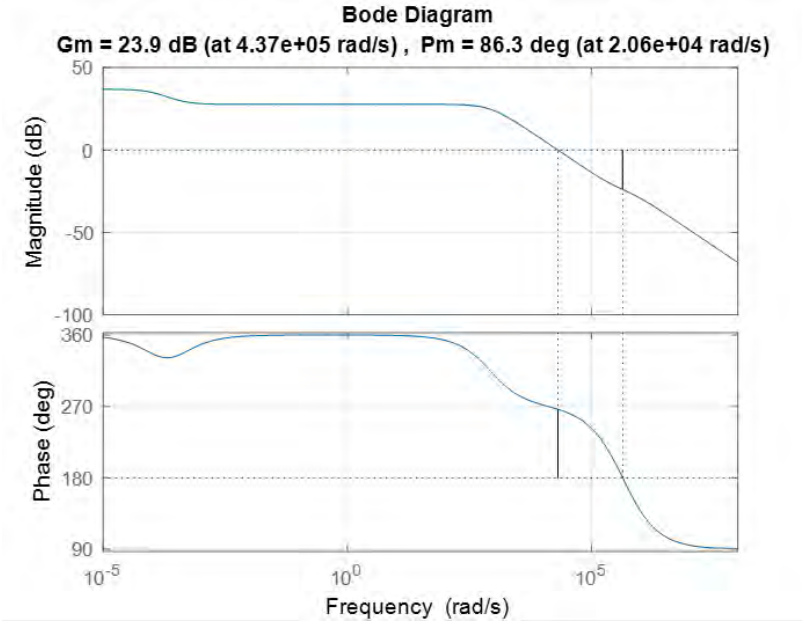

Figure 9. Bode plot of the output voltage transfer function

The voltage and current controller is a PI controller, the controller parameters are tuned manually, and they are shown in equations (13) and (14)

$$G_{cv} = 10 + \frac{10}{s} \tag{13}$$

$$G_{ci_o} = 7 + \frac{4}{s} \tag{14}$$

And the Bode plots of the open loop controlled plants are in Fig. 10 and Fig. 11.

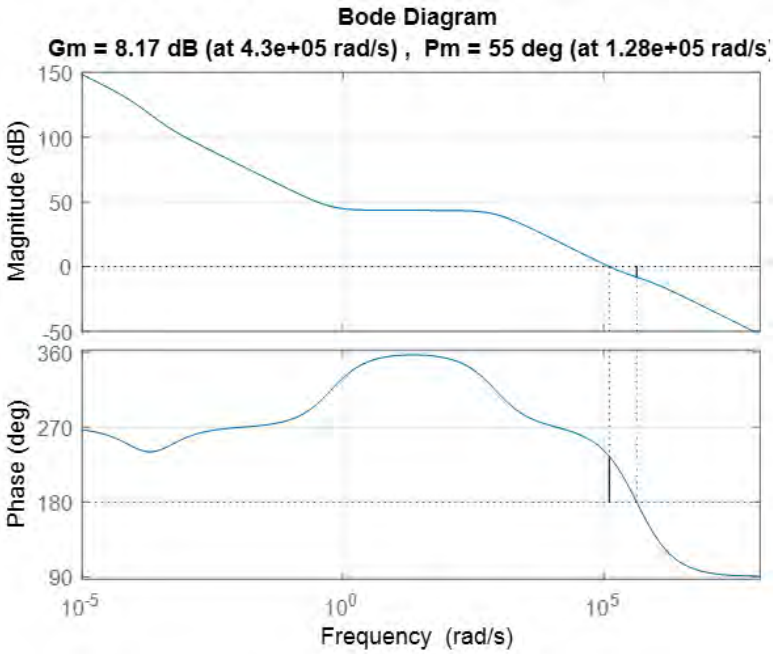

Figure 10. Bode plot of the open loop controlled output voltage transfer function

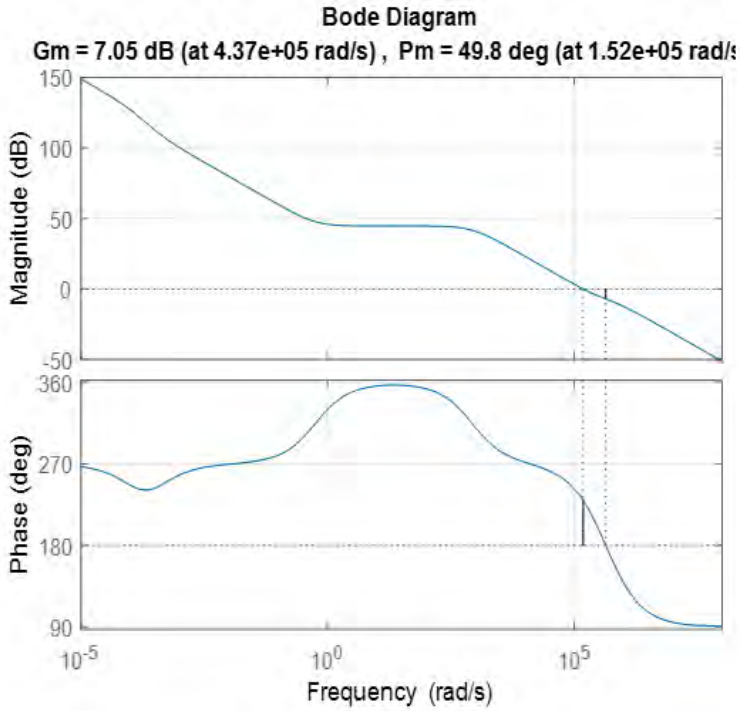

Figure 11. Bode plot of the open loop controlled output current transfer function

4. Simulation Results

The system specifications are shown in the table 1 below.

Table 1. System Specifications

TEG System	20 X TEG1-12611-6.0, 2S10P	V_D	0.35 V
V_s	5.2 − 12 V	C	3000 μF
R_s	0.193 − 0.225 Ω	R_c	0.0035 Ω
P_{TEG}	160 W	L_o	1μH
F_s	350 kHz	R_{Lo}	0.005 Ω
C_i	30 μF	Battery	*Samsung ICR*18650 6*S*2*P*
R_{ci}	0.005 Ω	Nominal voltage	22.2 V
L	2.5 μH	Full Charge Voltage	25.2 V
R_L	0.005 Ω	Nominal current	5.2 A
$R_{DS,ON}$	0.0025 Ω	R_b	0.6
R_D	0.004 Ω	C_b	4830 F
		Maximum charging current	5 A

Figure 12 shows the transition between the MPPT mode and the constant current mode when the generated current exceeds the battery limit at high hot side temperatures. As can be seen the current controller transition is seamless and no induced overshoots appear. Figure 13 shows that even during varying hot side temperature, constant current control is maintained if the generated current exceeds the battery recommended maximum limit. The transition between the constant current mode and the MPPT mode is held stable with the aid of small hysteresis band for the current as can be seen in Fig. 13, where the controller shifts to constant current mode whenever the charging current hits the upper limit of the hysteresis band set here to be 5.1 A, where the lower band is set to be 4.9 A. During MPPT mode and constant current mode, the battery voltage is rising up due to charging process and whenever the battery voltage is at its rated value, the controller shifts to constant voltage control as can be seen in Fig. 14 below. Fig. 15 shows how the constant voltage control is maintained during changes in the temperature gradient applied across the structure. The overshoot seen in the output voltage when shifting to constant voltage control from the constant current control or the MPPT control does not in fact exist when experimenting real system due the existence of the output capacitor which damps any changes in the output voltage. Table 2 below shows a summary of the findings of the simulation results.

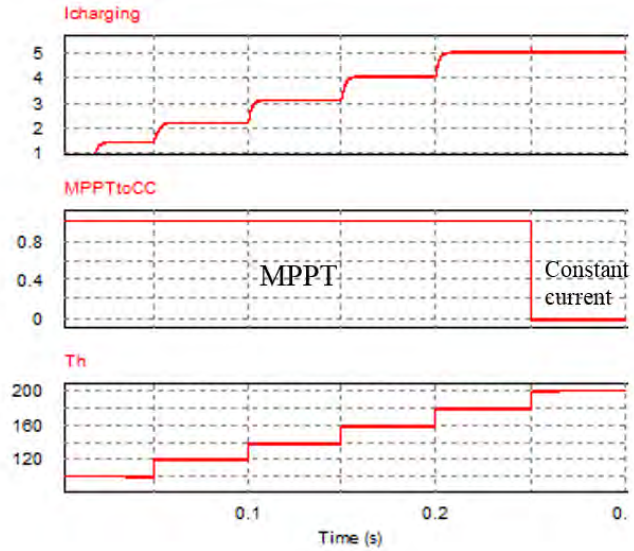

Figure 12. Output current at different hot side temperatures in the full operation range of 100°Cto 200 °C during current control stage

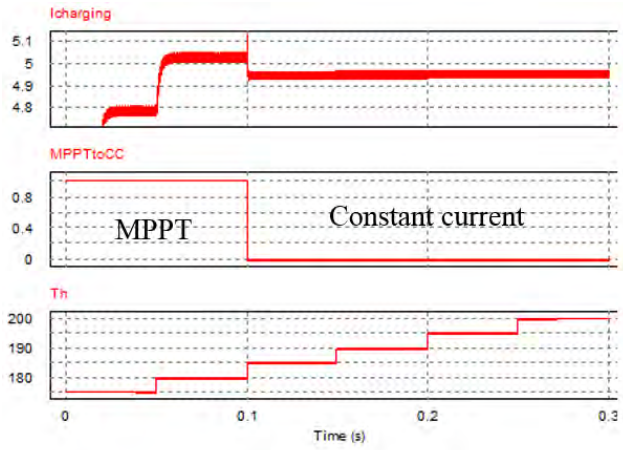

Figure 13. Output current at various hot side temperature values with constant current mode control.

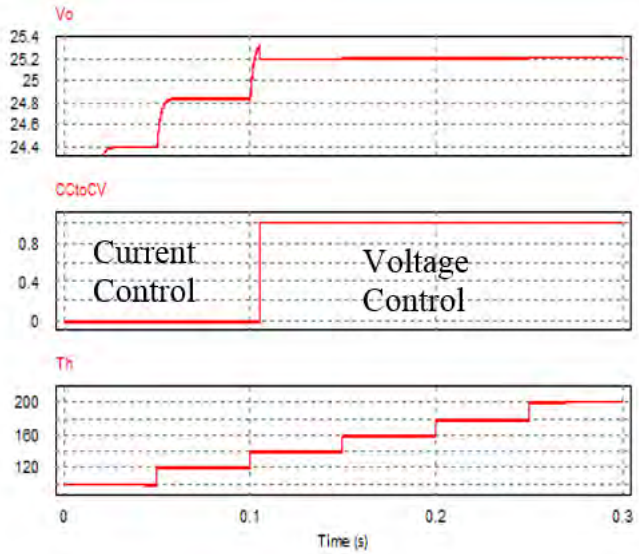

Figure 14. Output voltage at different hot side temperatures in the full operation range of 100°C to 200 °C during voltage control stage

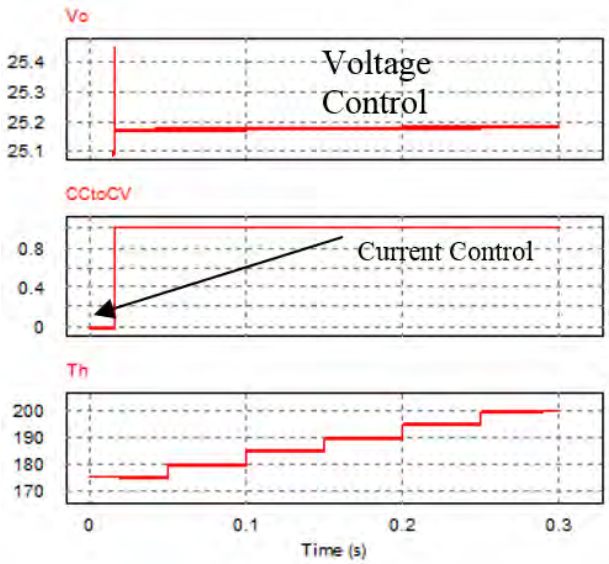

Figure 15. Output voltage at various hot side temperature values during voltage control stage

Table 2. Simulation Results

Output Voltage	25.171 - 25.234 V
Output current	4.978 - 5.017 A
Current ripple%	$< 1\%$
Voltage ripple%	$< 1\%$
Maximum output power	126.55 W
Efficiency	$\geq$93.6%

5. Conclusion

In this paper, a schematic design for energy harvesting from thermoelectric generators is put and simulated, where a commercial TEG product (TEG1-12611-6.0) is modeled using PSIM, and a commercial Battery (Samsung ICR18650) is modeled. Boost DC-DC converter topology is used. All components are supposed to be parasitic, and a smoothing inductor is used at the output. MPPT Perturb and Observe algorithm is combined with constant current/constant voltage in the charging controller to achieve the maximum possible power out of the TEG bank. Simulation results show that the proposed system operated at hot side temperatures range of 100-200oC and a cold side temperature of 30oC with a minimum efficiency of 93.6% and an output current and voltage ripple of less than 1%.

6. Acknowledgments

The authors would like to thank the German Jordanian University represented by the Deanship of Graduate Studies and Scientific Research for supporting this work.

7. References

1. R. R. Judkins, W. Fulkerson, and M. K. Sanghvi, "The dilemma of fossil fuel use and global climate change," *Energy & Fuels,* vol. 7, pp. 14-22, 1993/01/01 1993.

2. T. Mousseau and A. P. Møller, "Perspectives on Chernobyl and Fukushima Health Effects: What Can Be Learned From Eastern European Research?," *Journal of Health and Pollution,* vol. 3, pp. 2-6, 2013.

3. S. Kumar and O. Singh, "Performance Evaluation of Gas-Steam Combined Cycle Having Transpiration Cooled Gas Turbine," *Distributed Generation & Alternative Energy Journal,* vol. 28, pp. 43-60, 2013/04/01 2013.

4. D. Rowe, "Thermoelectric waste heat recovery as a renewable energy source," *Int. J. Innov. Energy Syst. Power,* vol. 1, pp. 13-23, 2006.

5. S. B. Riffat and X. Ma, "Thermoelectrics: a review of present and potential applications," *Applied Thermal Engineering,* vol. 23, pp. 913-935, 2003.

6. D. Rowe, "Thermoelectrics, an environmentally-friendly source of electrical power," *Renewable Energy,* vol. 16, pp. 1251-1256, 1999.

7. S. Dalola, M. Ferrari, V. Ferrari, M. Guizzetti, D. Marioli, and A. Taroni, "Characterization of Thermoelectric Modules for Powering Autonomous Sensors," *IEEE Transactions on Instrumentation and Measurement,* vol. 58, pp. 99-107, 2009.

8. F. Deng, H. Qiu, J. Chen, L. Wang, and B. Wang, "Wearable Thermoelectric Power Generators Combined with Flexible Super Capacitor for Low-power Human Diagnosis Devices," *IEEE Transactions on Industrial Electronics,* vol. PP, pp. 1-1, 2016.

9. H. Y. Won, Chae, S. Y., & Hong, S. C., ”State space averaging based analysis of the lithium battery charge/discharge system,” *The Transactions of the Korean Institute of Power Electronics,* vol. 14, p. 10, 2009.

10. V. T. VS Nguyen , W Choi , and DW Kim , “Analysis of the Output Ripple of the DC–DC Boost Charger for Li-Ion Batteries”, Journal of Power Electronics, vol. 1, no. 1, Jan 2014.

11. A. R. Reisi, Moradi, M. H., & Jamasb, S. “). Classification and comparison of maximum power point tracking techniques for photovoltaic system: A review”. Renewable and Sustainable Energy Reviews, 19, 433-443. 2013.

12. V. Vorperian, ”Simplified analysis of PWM converters using model of PWM switch. II. Discontinuous conduction mode,” *IEEE Transactions on Aerospace and Electronic Systems,* vol. 26, pp. 497-505, 1990.